Elastic moduli of muscovite mica

1993 J. Phys.: Condens. Matter 5 1681

(http://iopscience.iop.org/0953-8984/5/11/008)

J. Phys.: Condens. Matter 5 (1993) 1681–1690. Printed in the UK

Elastic moduli of muscovite mica

L E McNeil† and M Grimsditch‡

† Department of Physics and Astronomy, University of North Carolina at Chapel Hill, Chapel Hill, NC 27599-3255, USA

‡ Materials Science Division, Argonne National Laboratory, Argonne, IL 60439, USA

Received 8 October 1992, in final form 15 December 1992

Abstract. We have used Brillouin scattering to measure the thirteen independent elastic moduli of muscovite mica. The moduli reflect the monoclinic symmetry of the crystal, and demonstrate the anisotropy of the interlayer and intralayer bonding. The decrease in the acoustic velocity with increasing temperature is dominated by the decrease in the moduli that depend on interlayer bonding, giving an estimate of the temperature dependence of those moduli.

1. Introduction

Mica, the familiar layered silicate mineral, was once regarded as a natural resource of tremendous importance. In 1945, researchers for the (then) National Bureau of Standards declared it 'one of the most important strategic minerals in time of war, and indispensable in some modern applications in time of peace' [1]. While it has largely been replaced by other materials in its former applications in capacitors, airplane spark plugs, and the like, it continues to be used in ceramic composites and as an electrical insulator. In such applications the elastic properties of the crystal can play an important role.

The continuing interest in mica is nevertheless not based primarily on its usefulness, but on its characteristics as a highly anisotropic crystal. Like other layered materials such as graphite, transition-metal dichalcogenides and oxide superconductors, its properties are governed by the contrast between the strong intraplanar bonding and the much weaker interplanar forces. This anisotropy governs the mechanical properties as well as the optical and electrical characteristics, and is reflected most obviously in the easy cleavage parallel to the basal plane.

It is normally assumed that the elastic moduli will reflect the weak bonding along the cleavage planes, but furthermore the assumption is also often made that the *in-plane anisotropy will be small and that the material, though of a monoclinic* crystal structure, can be treated as possessing hexagonal symmetry. Existing elastic modulus data on muscovite are consistent with this expectation. However, because in a recent study of the monoclinic layered compound As_2S_3 [2] we found that the elastic moduli in no way reflect this 'expected' symmetry and that some of the in-plane moduli were actually smaller than the perpendicular ones, we undertook the present investigation of muscovite. We have used Brillouin scattering to measure the sound velocities, thereby obviating the difficulties typically encountered in performing ultrasonic measurements on fragile materials like mica.

0953-8984/93/111681+10$07.50

The many minerals under the general classification 'mica' consist of negatively charged silicate layers bonded together by interlayer cations [3]. Each layer consists of two tetrahedral sheets sandwiching one octahedral sheet, with apical oxygen atoms shared between the tetrahedral and octahedral sheets. The basal oxygens of the tetrahedral sheets form a hexagonal mesh on the outer surface of the layer, and the interlayer cations sit in the cavities at the centres of the six-membered rings.

Muscovite is a dioctahedral mica, i.e. of the three octahedra which form a repeat unit within the layer, two have octahedral cations (Al^{3+}) at their centres. The repulsion of the cations in adjacent octahedra leads to shifts and twists in the anion bonds, which break the biaxial symmetry of the layer [4]. One fourth of the tetrahedral cations are Al^{3+} rather than Si^{4+}, which gives a net negative charge to the layer and also expands the tetrahedral sheets, forcing the tetrahedra to rotate in the (001) plane to accommodate the smaller dimensions of the octahedral sheet. Potassium cations reside between the layers and bind them together, leading to the chemical formula $KAl_2(AlSi_3)O_{10}(OH)_2$. The cations in this formula are written in the order: interlayer cation–octahedral cation–tetrahedral cations. In the most common form of muscovite, the $2M_1$ polytype which is the subject of this study, successive layers are shifted laterally in alternating directions separated by 120°, leading to a monoclinic crystal structure with two layers per unit cell.

Crystals of monoclinic symmetry have 13 independent elastic moduli, namely C_{11}, C_{22}, C_{33}, C_{44}, C_{55}, C_{66}, C_{12}, C_{13}, C_{15}, C_{23}, C_{25}, C_{35}, and C_{46}. Of these, C_{11}, C_{22}, C_{66} and C_{12} are primarily dependent on the strong covalent bonding within the layers. The remaining moduli are governed by the weaker interlayer bonding, and should be more sensitive to perturbations caused by temperature, pressure, intercalation, and the like.

2. Experiment

The samples we used were large, transparent plates of natural muscovite, approximately 1 cm × 1 cm × 0.89 mm. We produced optical surfaces by cleaving the crystals with a razor blade, so the surfaces were (001) planes.

We made the Brillouin scattering measurements with a multipass tandem Fabry–Perot interferometer with 514.5 nm excitation from a single-mode Ar^+ laser. We used two scattering geometries: *backscattering*, in which the photons enter and exit on the same face of the crystal and the phonon propagates roughly perpendicularly to the crystal face; and *platelet*, in which incident and scattered photons enter and exit on opposite sides of a crystal with parallel surfaces, each at 45° to the crystal face. In this case the phonon propagates in the plane of the sample, and its direction in that plane can be varied relative to the crystal axes. For backscattering the phonon wavevector is given by $q = 2nk$ where n, the effective index of refraction of the medium, is an appropriate combination of the principal indices as dictated by the polarization of the incident and scattered light and k is the wavevector of the incident laser light. For the platelet geometry $q = \sqrt{2}k$ and is independent of n. For the backscattering measurements the Fabry–Perot operated in the 5 + 4 mode, and for the platelet measurements in the 3 + 2 mode.

We made high-temperature measurements in a furnace with the sample in air. The temperature, measured with a type K thermocouple, was stable to a precision of ±3 °C. Upon heating above 500 °C the samples took on a silvery black colour, which made measurements at higher temperatures impossible.

3. Results

3.1. Room temperature

The Brillouin frequency shifts ν (frequencies of the acoustic phonons) are converted to effective elastic moduli C_{eff} according to the usual expression

$$C_{\text{eff}} = \rho v^2 = \rho \left(\frac{\nu}{q}\right)^2 \tag{1}$$

where v is the sound velocity, q is the phonon wavevector defined in the previous section, and we have calculated the density $\rho = 2.832$ g cm^{-3} using the unit cell parameters [5]. For backscattering measurements we used values of the indices of refraction $n_a = 1.552$, $n_b = 1.582$ [6].

In the backscattering measurements in the a–c plane, which are restricted to propagation directions close to the normal of the cleavage planes, we typically observed three modes as shown in figure 1(*a*). Two of these modes are of quasilongitudinal and quasitransverse character and depend upon six of the thirteen independent elastic moduli: C_{11}, C_{33}, C_{55}, C_{13}, C_{15} and C_{35}. The third mode is of pure transverse character and depends upon the three elastic moduli C_{44}, C_{66} and C_{46}.

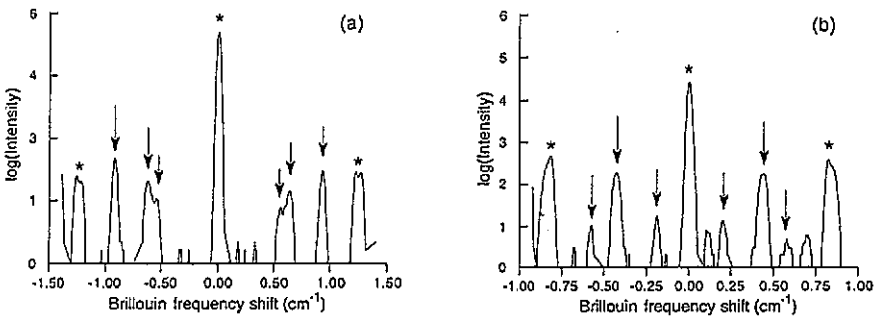

Figure 1. Typical Brillouin scattering spectra for two scattering geometries. Both Stokes and anti-Stokes spectra are shown and the Brillouin scattering peaks are marked with arrows. The peaks marked * arise from the unshifted laser light in zero and first order. (*a*) Backscattering geometry with phonon propagation in the a–c plane at an angle of 19° from the c axis. (*b*) Platelet geometry with phonon propagation in the a–b plane at 45° from the a axis.

The platelet measurements, in which the phonon propagates in the a–b plane, yield three modes of mixed character. A typical spectrum is shown in figure 1(*b*). These modes depend on nine elastic moduli: C_{11}, C_{22}, C_{44}, C_{55}, C_{66}, C_{12}, C_{15}, C_{25} and C_{46}. A description of how the relationship between the measured effective elastic modulus and the individual independent moduli is derived is presented in the appendix. Together the a–c and a–b plane measurements involve twelve of the thirteen moduli, omitting only C_{23}. This thirteenth modulus appears in the corresponding expressions for scattering in the b–c plane.

We have extracted the values of twelve of the elastic moduli from the a–c and a–b plane data via a non-linear least-squares fitting scheme using the program LEVM

[7]. We fit each set of frequencies to the appropriate propagation direction-dependent expression for C_{eff}, varying the elastic moduli as parameters until we obtained the best fit for all the data simultaneously. The weighting exponent was initially used as a free parameter, but when a value very close to 0.5 was obtained the final fits were done with the exponent fixed at 0.5 (in a counting experiment this would correspond to Poisson statistics). The uncertainties are taken from the standard deviations of the fit. The results of the fits are shown in figures 2 and 3, and the values we obtain are given in table 1. The b–c plane data (the only set which involves C_{23}) showed greater scatter and were used only to extract a somewhat more approximate value of the final modulus. This was accomplished by holding C_{22}, C_{33}, C_{44}, C_{55}, C_{66}, C_{25}, C_{35} and C_{46} fixed and varying only C_{23}. The best value obtained appears in the table.

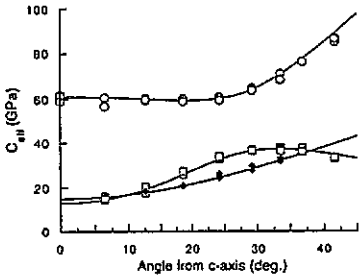

Figure 2. Effective elastic modulus C_{eff} for propagation in the a–c plane, as a function of the angle between the direction of propagation and the c axis. The lines are fits to the data as described in the text.

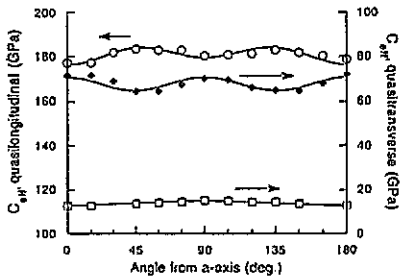

Figure 3. Effective elastic modulus C_{eff} for propagation in the a–b plane, as a function of the angle between the direction of propagation and the a axis. The lines are fits to the data as described in the text.

Table 1.

Elastic modulus	Value (GPa)
C_{11}	176.5±1.1
C_{22}	179.5±1.3
C_{33}	60.9±0.6
C_{44}	15.0±0.3
C_{55}	13.1±0.2
C_{66}	70.7±0.6
C_{12}	47.7±1.2
C_{13}	20.0±1.1
C_{15}	−1.2±0.6
C_{23}	23.0±8
C_{25}	11.1±5.3
C_{35}	−0.7±0.5
C_{46}	0.7±0.5

3.2. Elevated temperatures

We have measured the Brillouin frequency shift as a function of temperature in the backscattering geometry in the a–c plane with the phonon propagation direction

inclined at 24° from the c axis inside the crystal. For propagation in this direction all three modes are observable. We have also taken measurements for propagation along the c axis, for which only the longitudinal mode is observed. The variation of this frequency with temperature was identical to that of the longitudinal mode at 24°.

In order to calculate the effective elastic constant from the frequency shift, the values of the density ρ and refractive index n as a function of temperature are required. Typical thermal expansion coefficients perpendicular to the cleavage plane recorded for muscovite mica [1] are in the range $\alpha_\perp = 13\text{–}17 \times 10^{-6}\,°C^{-1}$ in the temperature range 20–300 °C, and $16\text{–}24 \times 10^{-6}$ over 300–600 °C. Parallel to the cleavage plane the same source reports values of $\alpha_\parallel = 8.0\text{–}12 \times 10^{-6}\,°C^{-1}$ in the same temperature range, with the coefficient increasing with temperature. The expansion perpendicular to the plane is thus approximately twice that parallel to the plane at all temperatures. We have used the average values for the expansion reported for each temperature range, and taken

$$\mathrm{d}\ln\rho/\mathrm{d}T = -(2\mathrm{d}\alpha_\parallel/\mathrm{d}T + \mathrm{d}\alpha_\perp/\mathrm{d}T). \tag{2}$$

To correct the index of refraction we have used the simple Lorentz–Lorenz formula $(n^2-1)/(\rho(n^2+2)) =$ constant. Although it may appear that the uncertainties in the thermal expansion coefficients and the simplicity of the Lorentz–Lorenz correction could lead to large errors, since neither of the corrections exceeds $\sim 2\%$ the uncertainties in the corrections lead to negligible errors. Including both corrections (which are of opposite sign in their effects on the modulus) we obtain the values shown in figure 4. The quasilongitudinal mode, which is dominated by C_{33} at this angle, decreases linearly with increasing temperature with a slope of -1.2×10^{-2} GPa °C^{-1}. The pure transverse mode, which is dominated by C_{44}, behaves similarly with a slope of -7.2×10^{-3} GPa °C^{-1}. The quasitransverse mode, which depends on the intraplane bonding, has the smallest slope of -2.3×10^{-3} GPa °C^{-1}. The lines shown in figure 3 result from the assumption that the variation with temperature of the modes can be accounted for by changes in C_{33}, C_{13}, C_{44} and C_{55}. By setting the temperature derivatives of these four moduli equal to -8.0×10^{-3} GPa °C^{-1} and calculating C_{eff} at each temperature, we obtain the lines shown in the figure. The exact values of the temperature derivatives should not be taken too seriously, since the complicated dependence of the frequencies on the elastic moduli does not allow individual moduli to be obtained separately from measurements for a single propagation direction. However, they do show that the changes in the elastic wave velocities with temperature can be attributed primarily to changes in those moduli that depend on the bonding between, rather than within the layers of the crystal.

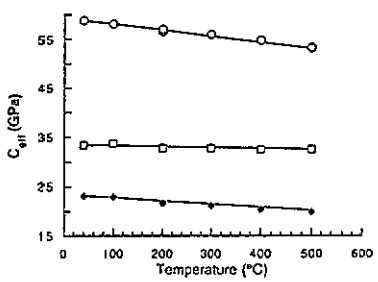

Figure 4. Effective elastic modulus C_{eff} for propagation in the a–c plane at an angle of 24° to the c axis, as a function of temperature. The lines are calculated by setting the temperature derivatives of C_{33}, C_{13}, C_{44} and C_{55} equal to -8.0×10^{-3} GPa °C^{-1} (see text).

We have also made temperature-dependent measurements in the platelet geometry for a single propagation direction, but the scatter in the results and the greater complexity of the relations between the mode frequencies and the elastic moduli make detailed analysis difficult. The effective elastic moduli did decrease by about 5% in 500 °C, consistent with the changes in C_{44} and C_{55} obtained from the backscattering results. It is worth noting that the index of refraction does not enter into the platelet results.

4. Discussion

4.1. Room temperature

There appear to have been no previous Brillouin scattering measurements reported for mica, but a few studies of acoustic phonons and of elasticity have been made using neutron scattering and mechanical methods. Wada and Kamitakahara [8] used inelastic neutron scattering to determine the acoustic velocities along the c and b axes of muscovite. In the c direction they obtained values of 4.1×10^5 cm s^{-1} for the longitudinal wave and 2.4×10^5 cm s^{-1} for the transverse wave, with an estimated error of 10–15% due to a paucity of data at low energies at the zone centre. These compare well with the values we have obtained by Brillouin scattering (which of course probes exactly the region of reciprocal space that is difficult to observe with neutron scattering). For the quasilongitudinal wave along c we obtain a velocity of 4.54×10^5 cm s^{-1}. In exact backscattering this is the only observable mode, but at an angle of 12.5° from the c axis inside the crystal in the c–a plane all three modes are observable. In this direction the quasitransverse and pure transverse wave velocities are 2.66×10^5 cm s^{-1} and 2.48×10^5 cm s^{-1}, also in good agreement with the neutron results. In the platelet geometry we have measured the velocity of acoustic phonons propagating along the b axis, and our values for the three modes are 7.98×10^5 cm s^{-1}, 4.98×10^5 cm s^{-1}, and 2.31×10^5 cm s^{-1}, which are to be compared to Wada and Kamitakahara's values of 7.5×10^5 cm s^{-1} and 4.5×10^5 cm s^{-1}. They found the frequency of the lower-energy transverse mode to have a non-linear dependence on q, and therefore did not calculate a velocity. This non-linearity is characteristic of the so-called 'flexural' mode in layered materials [9]. The velocity of the quasilongitudinal mode along the c axis was earlier measured by Cebula *et al* [10] using the same technique, obtaining a value of $4.5 \pm 0.2 \times 10^5$ cm s^{-1}, in agreement with our result and with that of Wada and Kamitakahara.

Alexandrov and Ryzhova [11] (using ultrasonic techniques) and Caslavsky and Vedam [12] (using flexure) measured the elastic moduli of muscovite. Both groups found no anisotropy of the elastic moduli in the basal plane (the latter workers achieving this result only for samples free of layer corrugations as measured by Bragg diffraction), indicating that the symmetry of the elastic behaviour was hexagonal. The values obtained by Alexandrov and Ryzhova, $C_{11} = 178$ GPa, $C_{33} = 54.9$ GPa, $C_{44} = 12.2$ GPa, $C_{12} = 42.4$ GPa and $C_{13} = 14.5$ GPa, are not very different from our Brillouin scattering values for these moduli. At least some of the difference may arise from their assumption of hexagonal symmetry, which neglects the contribution of other moduli which are non-zero in a monoclinic crystal. For example, the average of C_{11} and C_{22} from our Brillouin measurements gives exactly the Alexandrov and Ryzhova value for C_{11}.

The first observation that one can make about the elastic moduli we have obtained is that they do indeed reflect the monoclinic symmetry of the muscovite crystal, which is well established from x-ray diffraction. However, the anisotropy within the basal plane is small, which may explain why it was not observed in earlier elasticity measurements. While C_{11} and C_{22} differ by barely more than one standard deviation, the values of C_{44} and C_{55}, which would also be equal if the basal plane were elastically isotropic, differ by considerably more. The two pairs are also in the same relation, i.e. $C_{11} < C_{22}$ and $C_{55} < C_{44}$, as would be expected. Also as expected $C_{13} < C_{23}$ but the two values are similar. The moduli that would vanish if the symmetry were hexagonal, i.e. C_{15}, C_{25}, C_{35} and C_{46}, all differ from zero by more than one standard deviation, and by at least two standard deviations in the case of C_{15} and C_{25}. C_{66}, which for hexagonal symmetry would be equal to $(C_{11} - C_{12})/2$, differs significantly from this value even if the average of C_{11} and C_{22} is used instead of the smaller C_{11}. In this case we would obtain $C_{66}^{\text{hex}} = 65.2$ GPa, compared with the measured value of 70.7 ± 0.6 GPa. It is therefore clear that although the elastic anisotropy within the plane is small, the monoclinic symmetry of the crystal is reflected in the elastic moduli.

Contrary to the behaviour previously reported for As_2S_3, the basal plane of mica is relatively elastically isotropic. Furthermore, mica exhibits the elastic anisotropy between the in-plane and out-of-plane directions anticipated from the cleavage behaviour of the crystal. The nearly 300% difference between C_{11} or C_{22} and C_{33} arises from the difference between the strong covalent bonding within the silicate layer and the largely ionic bonding that holds the layers together. This is also apparent in the even larger difference in the shear moduli: C_{66} is approximately five times C_{44} or C_{55}.

4.2. Elevated temperatures

Much of the decrease with temperature in the moduli which involve interplanar bonding can be attributed to the thermal expansion which, as noted above, is dominated by expansion in the direction perpendicular to the plane. With anharmonicity present, this increased separation of the layers will necessarily decrease the force constants of the bonding between them, and thus decrease the corresponding vibrational frequencies and elastic moduli. In a quasiharmonic model of lattice vibrations the leading term in the temperature-dependent elastic moduli is expected to be linear in T [13], with a slope that depends on the particular modulus and on the Debye temperature of the material. The fact that the greatest declines in the moduli with increasing temperature are in those that involve interlayer coupling is not surprising, given that the greatest increase in interatomic spacing takes place between the layers.

The magnitude of the logarithmic decrease in the interlayer elastic moduli with temperature, roughly $2.5 \times 10^{-4}\,°C^{-1}$, is somewhat larger than that observed in simpler oxide minerals. For example, in Al_2O_3 the compressional moduli C_{11} and C_{33} decrease by approximately $0.9 \times 10^{-4}\,°C^{-1}$, and C_{44} by roughly $1.5 \times 10^{-4}\,°C^{-1}$ [14]. In orthorhombic forsterite (Mg_2SiO_4) the logarithmic derivatives range from $d(\ln C_{23})/dT = -0.6 \times 10^{-4}\,°C^{-1}$ to $d(\ln C_{66})/dT = -2.0 \times 10^{-4}\,°C^{-1}$ [15]. The values for cobalt olivine, Co_2SiO_4 are similar, falling in the even more narrow range -1.1 to $-1.8 \times 10^{-4}\,°C^{-1}$. The above comparison is also consistent with the changes in interatomic spacing with temperature, since in these minerals the linear thermal expansion coefficients are in a range similar to or smaller than $\alpha_{\|}$ of muscovite.

5. Summary

We have used Brillouin scattering to measure the thirteen independent elastic moduli of muscovite mica. The values of the moduli exhibit the monoclinic structure of the crystal and reflect the anisotropy between the interlayer and intralayer bonding. The temperature dependence of the moduli is dominated by the decrease in the interplanar bonding as the spacing between the layers increases.

Acknowledgments

We are grateful to K Bradley for providing the samples used in this study, and to J Ross Macdonald for assistance with the numerical analysis. One of us (LEM) would like to thank the University of North Carolina Arts and Sciences Foundation for partial support of this work. The measurements at Argonne National Laboratory were supported by the US Department of Energy, BES-Materials Sciences under contract #W-31-109-ENG-38.

Appendix

The relationship between the modulus C_{eff} measured by Brillouin scattering and the individual independent elastic moduli depends on the direction of propagation of the phonon and on the symmetry of the crystal. The equations of motion for the crystal, together with the restrictions imposed by symmetry, result in a matrix involving the effective modulus and the direction cosines along the principal axes of the crystal. The eigenvalue equations for this matrix are the Christoffel equations, the solutions of which give the desired relation between C_{eff} and the individual moduli C_{ij} as a function of the propagation direction. A detailed treatment of this subject can be found in any standard reference on elasticity and crystal symmetry [16].

For the specific case of propagation in the a–c plane, corresponding to our backscattering geometry measurements, the mathematics yields a quadratic equation and a linear one. The solutions correspond in the first case to a quasilongitudinal and a quasitransverse wave and in the second to a pure transverse mode. The quadratic equation yields effective moduli of the form:

$$C_{\text{eff}}^{\pm} = \tfrac{1}{2}(-b \pm \sqrt{b^2 - 4c}) \tag{A1}$$

where the quadratic coefficients b and c depend upon the individual moduli and are functions of the angle θ between the propagation direction of the phonon and the c axis

$$b = -[\sin^2\theta(C_{11} + C_{55}) + 2\sin\theta\cos\theta(C_{15} + C_{35}) + \cos^2\theta(C_{33} + C_{55})] \tag{A2}$$

$$\begin{aligned} c = {} & \sin^4\theta(C_{11}C_{55} - C_{15}^2) + 2\sin^3\theta\cos\theta(C_{11}C_{35} - C_{13}C_{15}) \\ & + \sin^2\theta\cos^2\theta(C_{11}C_{33} - C_{13}^2 + 2C_{15}C_{35} - 2C_{13}C_{55}) \\ & + 2\sin\theta\cos^3\theta(C_{33}C_{15} - C_{13}C_{35}) \\ & + \cos^4\theta(C_{33}C_{55} - C_{35}^2). \end{aligned} \tag{A3}$$

The linear equation for the pure transverse mode has as its solution

$$C_{\text{eff}} = C_{66}\sin^2\theta + C_{44}\cos^2\theta + 2C_{46}\sin\theta\cos\theta. \tag{A4}$$

The a–c plane backscatter frequencies therefore depend on nine of the thirteen independent elastic moduli: C_{11}, C_{33}, C_{44}, C_{55}, C_{66}, C_{13}, C_{15}, C_{35} and C_{46}.

For propagation in the a–b plane, corresponding to our platelet geometry measurements, the effective elastic moduli are the roots of a cubic equation of the form

$$C_{\text{eff}}^3 + \alpha C_{\text{eff}}^2 + \beta C_{\text{eff}} + \gamma = 0 \tag{A5}$$

with coefficients

$$\alpha = -[\cos^2\theta(C_{11} + C_{55}) + \sin^2\theta(C_{22} + C_{44}) + C_{66}] \tag{A6}$$

$$\begin{aligned}\beta = [&\cos^4\theta(C_{11}C_{55} + C_{11}C_{66} + C_{55}C_{66} - C_{15}^2)\\ &+ \cos^2\theta\sin^2\theta(C_{11}C_{22} + C_{11}C_{44} + C_{22}C_{55} + C_{44}C_{66}\\ &+ C_{55}C_{66} - C_{12}^2 - C_{25}^2 - C_{46}^2 - 2(C_{15}C_{46} + C_{25}C_{46} + C_{12}C_{66}))\\ &+ \sin^4\theta(C_{22}C_{44} + C_{22}C_{66} + C_{44}C_{66} - C_{46}^2)]\end{aligned} \tag{A7}$$

$$\begin{aligned}\gamma = -[&\cos^6\theta(C_{11}C_{55}C_{66} - C_{66}C_{15}^2)\\ &+ \cos^4\theta\sin^2\theta(2C_{12}C_{15}C_{25} + 2C_{12}C_{15}C_{46} - 2C_{11}C_{25}C_{46} - C_{22}C_{15}^2\\ &- C_{11}C_{25}^2 - C_{11}C_{46}^2 + C_{11}C_{22}C_{55} + 2C_{66}C_{15}C_{25} + C_{11}C_{44}C_{66}\\ &- 2C_{55}C_{66}C_{12}) + \cos^2\theta\sin^4\theta(C_{11}C_{22}C_{44}\\ &- C_{44}C_{12}^2 - 2C_{22}C_{15}C_{46} + 2C_{12}C_{25}C_{46}\\ &+ 2C_{12}C_{46}^2 - C_{66}C_{25}^2 - 2C_{44}C_{66}C_{12}\\ &+ C_{22}C_{55}C_{66}) + \sin^6\theta(C_{22}C_{44}C_{66} - C_{22}C_{46}^2)].\end{aligned} \tag{A8}$$

Here θ is the angle between the phonon propagation direction and the a axis. These also depend upon nine of the thirteen independent elastic moduli: C_{11}, C_{22}, C_{44}, C_{55}, C_{66}, C_{12}, C_{15}, C_{25} and C_{46}. A similar cubic equation involving C_{22}, C_{33}, C_{44}, C_{55}, C_{66}, C_{25}, C_{35}, C_{46} and C_{23} is obtained for backscattering measurements in the b–c plane, so all thirteen of the moduli can be determined from the three experiments.

References

[1] Hidnert P and Dickson G 1945 *J. Res. Nat. Bur. Std.* 35 309

[2] McNeil L E and Grimsditch M 1991 *Phys. Rev.* B 44 4174

[3] Bailey S W 1984 Classification and Structures of the Micas *Micas, Rev. Mineral.* vol 13, ed S W Bailey (Washington, DC: Mineralogical Society of America)

[4] Bailey S W 1984 Crystal Chemistry of the True Micas *Micas, Rev. Mineral.* vol 13, ed S W Bailey (Washington, DC: Mineralogical Society of America)

[5] Wyckoff R W G 1971 *Crystal Structures* 2nd edn (New York: Interscience)

[6] Wilcox R E 1984 Optical Properties of Mica under the Polarizing Microscope *Micas, Rev. Mineral.* vol 13, ed S W Bailey (Washington, DC: Mineralogical Society of America)

[7] Macdonald J R and Potter L D Jr 1987 *Solid State Ionics* 23 68
Macdonald J R 1990 *Electrochimica Acta* 35 1483

[8] Wada N and Kamitakahara W A 1991 *Phys. Rev.* B **43** 2391
[9] Belen'kii G L, Salaev É Yu and Suleimanov R A 1988 *Sov. Phys. Usp.* **31** 434
[10] Cebula D J, Owen M C, Skinner C, Stirling W G and Thomas R K 1982 *Clay Minerals* **17** 195
[11] Alexandrov K S and Ryzhova T V 1961 *Izm. Akad. Nauk. SSSR, Ser. Geofiz.* **1961** 1339
[12] Caslavsky J L and Vedam K 1970 *Am. Mineralogist* **55** 1633
[13] Anderson O L 1966 *Phys. Rev.* **144** 553
[14] Zouboulis E S and Grimsditch M 1991 *J. Appl. Phys.* **70** 772
[15] Hellwege K-H and Madelung O (ed) 1979 *Landolt–Börnstein Numerical Data and Functional Relationships in Science and Technology* vol III/11 (Berlin: Springer)
[16] Hellwege K-H and Madelung O (ed) 1984 *Landolt–Börnstein Numerical Data and Functional Relationships in Science and Technology* vol III/18 (Berlin: Springer)
[17] Nye J F 1985 *Physical Properties of Crystals* (Oxford: Oxford University Press)
Mason W P 1958 *Physical Acoustics and the Properties of Solids* (Princeton: Van Nostrand)
Love A E H 1927 *A Treatise on the Mathematical Theory of Elasticity* 4th edn (Cambridge: Cambridge University Press)